2008 IEEE International Conference on
Robotics and Automation
Pasadena, CA, USA, May 19-23, 2008

Performance of Different Foot Designs for a Water Running Robot

Steven Floyd[†*], Serhat Adilak[‡], Steven Ramirez[*], Raphael Rogman[*], and Metin Sitti[*]

Abstract— **The water runner robot is designed to run on the surface of water in a manner similar to the basilisk lizard. To do so, it must generate a lift force greater than its weight by slapping and stroking its foot through the water, creating an air cavity in the process. In addition, it must remove its foot before this cavity collapses. Basilisk lizards deal with this problem by folding their feet during retraction from the air cavity to avoid prematurely collapsing the cavity and generating excess drag. Several different passive foot designs for the water runner were analyzed to determine which had the largest lift and created the least amount of drag. Feet with folding sections which collapse during retraction and spring back into place once the foot has exited the water were found to work best. Those feet which allowed air to pass through during retraction provided the least net lift. Elliptic feet with their major axis in line with the direction of running performed better than simple circular feet. Consequences of these results are discussed.**

I. INTRODUCTION

Small, lightweight animals have a large variety of flotation mechanisms available to them. There are spiders and insects which float using surface tension [1], [2], propel themselves using menisci in the water [3], and secrete surfactants to move utilizing marangoni flows. Larger animals have fewer options. Lizards, aquatic birds, and marine mammals, with their larger bulk and higher mass, utilize buoyancy, viscous drag and momentum transfer [4].

The basilisk lizard (*Basiliscus* sp.) is capable of running across the surface of water at approximately 1.5 m/s, in excess of 10 body lengths per second, at a stepping rate of 5-10 Hz (per leg) [5]. Four factors influence the lizard's ability to stay afloat: a) body mass, b) characteristic length, c) running speed, and d) shape of the foot. All of these variables are inter-related, and the morphological relations to the lizard's water running have been characterized in [5]–[9].

Biomimetic robots are those machines which emulate some aspect of a living system. In this case, the ability to run over water is what our robot attempts to duplicate. Unlike other aquatic and amphibious robots which must swim or walk through the water [10]–[13], the water runner can stride upon it. This robot employs momentum transfer for both lift and propulsion, instead of surface tension or buoyancy which other water walking robots employ [2], [14], [15]. Hence, the robot will be the lightest of the amphibious robots, but the heaviest of the water walkers. The goal is not to copy nature, but to understand the principles of operation, and use or improve on them for use in our own creations.

Previous work on this subject has focused on generating theoretical models to examine the robot's ability to generate lift and the corresponding power consumption [16]. Parameters that were examined included characteristic length, running speed, foot diameter and orientation relative to the leg. This paper's goal is to analyze both qualitatively and quantitatively the effect of different foot designs on the generation of lift and drag.

Other authors have created a theoretical model with which one can treat the lizard's foot as a circle for the purposes of examining the forces generated [6]–[8]. But, fundamentally, the lizard's foot is not a simple, passive circle. It is an actuated, dynamically changing limb which is actively used to generate forces and increase stability [5], [9]. Because of limitations in terms of weight and power consumption, simple and passive limbs must be used on the water runner. So many of the actions a lizard's foot makes during the process of water running must be ignored, or replicated as effectively as possible without the use of muscles.

II. FOOT AND WATER INTERACTIONS

Similar to the lizard, to create lift and forward thrust the robot strikes its foot into the water and pulls toward the rear. To accomplish this motion, the water runner uses four bar mechanisms as legs. The choice of four bar link lengths was described in previous works [16]. A simple schematic of the water runner is shown in Fig. 1. Four legs are used on the water runner instead of the lizard's two for stability reasons.

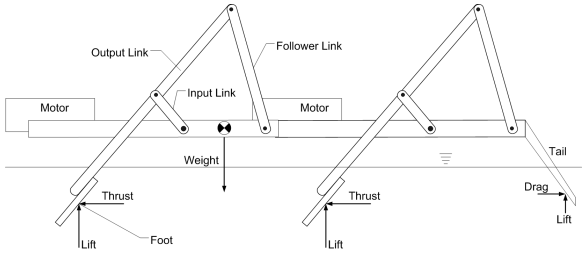

Fig. 1. Schematic of the four legged water runner as seen from the side. Each leg is a four bar mechanism.

Each input link is connected to a motor via a pair of bevel gears. These turn at a constant rate and cause the foot to follow a smooth path through space. For each leg, the foot is located at the far end of the output link. The follower link rocks back and forth through a limited angular range.

[†] Corresponding author, srfloyd@andrew.cmu.edu
[*] Department of Mechanical Engineering, Carnegie Mellon University, Pittsburgh, PA 15213, USA
[‡]Mechatronics Engineering, FENS, Sabanci University, Tuzla 34956, Istanbul, Turkey

A. Water Entry

The forces experienced by a disk entering water vertically and creating an air cavity are described at length by others [6]. In summary, there are two distinct phases that occur before the cavity collapses: the slap and stroke phases [6]–[8]. The slap phase is characterized by high impact forces over a short period of time. Disk motion is primarily downward, and the magnitude of the impulse force is a function of the disk's radius and velocity:

$$I_{slap}^{max} = \frac{4}{3}\rho r^3 u_{peak} \tag{1}$$

where I_{slap}^{max} is the maximum slap impulse transferred to the disk, ρ is the density of water, approximately 997 kg/m^3, r is disk radius, and u_{peak} is the peak velocity during the slap.

The stroke phase begins just after the initial slap. Drag on the foot is a combination of hydrostatic drag due to increasing depth and inertial drag from momentum transferred to the fluid. The governing equation for the stroke phase is:

$$D(t) = C_D^*[0.5S\rho u^2 + S\rho g h(t)] \tag{2}$$

where $D(t)$ is the time varying drag force, $C_D^* \approx 0.703$ is the constant drag coefficient [6], g is acceleration due to gravity, $S = \pi r_{eff}^2$ is the circular area over which drag is occurring, and $h(t)$ is the time varying depth of the disk.

B. Retraction

At high cycling rates, an air cavity is formed by the path the robot's foot takes through the water during the slap and stroke phases. To avoid being submersed in the water, the robot, like the lizard, must remove its foot from the air cavity before it collapses. The time required for the cavity to collapse is nearly independent of the foot's velocity, and is purely a function of the foot's radius r. From that collapse period, a minimum frequency f_{min} can be determined if one assumes that the robot's leg spends about half the time in the water. The cavity collapse time (T_{seal}) and minimum frequency were found [6] for circular disks to be:

$$T_{seal} = 2.285\sqrt{\frac{r_{eff}}{g}} \tag{3}$$

$$f_{min} = \frac{1}{2T_{seal}} \tag{4}$$

When pulling its foot out of the water during retraction, the basilisk lizard will curl its toes inward to prevent accidental drag on the cavity walls and premature cavity collapse [9]. A rigid, flat, circular foot, like the kind first used on the water runner robot, is incapable of doing this. Various foot designs were compared to flat circular feet in terms of lift and drag in an attempt to reduce the negative effects which occur from using passive, simple feet on the water runner.

III. EXPERIMENTAL SETUP

To study the time varying forces experienced by one foot on the water runner robot, the system shown in Fig. 2 was built. A four bar mechanism suppresses lateral motion, while transmitting vertical forces from the robot to a cantilever beam. Along the way, these forces are amplified by a factor of four using a lever arm. The beam's deflection is measured using a Keyence LS-3034 laser micrometer, which is read by a Keyence LS-3100 Laser Scan Controller. Measurements from the laser micrometer are acquired at 1.0 KHz on a computer. Only one leg, the front left, is used for the lift experiments.

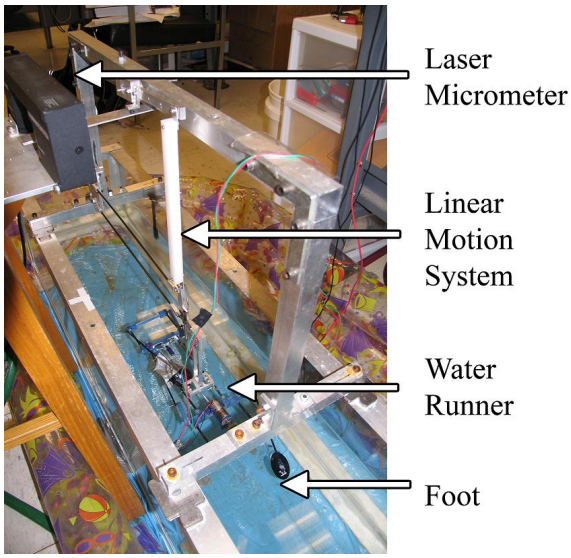

Fig. 2. Photograph of the experimental setup with components labeled. The linear motion system is composed of the four bar mechanism, a solid vertical beam, the lever arm used to amplify forces, and the cantilevered beam whose deflection is measured by the laser micrometer.

IV. VIBRATORY RESPONSES

The motion of the water runner's foot is cyclic, and repeats itself for every revolution of the input link. Because of this cyclic, repeating nature, the forces experienced by the robot can be accurately modeled as a sum of sines and cosines with varying amplitudes at the frequency of rotation of the input link and at integer multiples of this base frequency. The transformation from a time based, periodic signal to a summation of sines and cosines at various frequencies is accomplished via the Fourier Transform. For discrete data points, as when a real signal is measured by a computer, the Discrete Fourier Transform (DFT) is used. So long as the sampling frequency is much greater than the highest frequency of interest, the DFT can accurately capture the behavior of a periodic signal [17]–[19].

When the robot's foot interacts with the water, it creates periodic forces which are transmitted through the experimental setup to affect the deflection of the cantilever beam. For any real system, sines and cosines at different frequencies will experience different attenuations and phase shifts [20].

This causes signal distortion when measured by the laser micrometer and must be taken into account during processing.

To account for these distortions, the entire measurement system is modeled as a spring-mass-damper system. The characteristic equation for such a system is:

$$\ddot{x} + 2\zeta\omega_n\dot{x} + \omega_n^2 x = \frac{f(t)}{m} \tag{5}$$

where x is the displacement of the cantilever beam as measured by the laser micrometer, ζ is the damping ratio of the linear motion system, ω_n is the natural frequency of the system, and $f(t)$ is the force experienced by the water runner, a sum of cosines at various amplitudes and phases.

For a spring-mass-damper system, the amplitude attenuation and phase shift associated with sinusoidal forces are:

$$|x| = \frac{|f|}{m\sqrt{(\omega_n^2 - \omega^2)^2 + (2\zeta\omega_n\omega)^2}} \tag{6}$$

$$\phi = tan^{-1}\left(\frac{2\zeta\omega_n\omega}{\omega_n^2 - \omega^2}\right) \tag{7}$$

where ϕ is the phase lag of the output relative to the input. By measuring the step and impact response of the linear motion system, the system parameters of ω_n and ζ were found to be approximately $2\pi \times 54.3$ radians per second and 0.015, respectively.

V. EXPERIMENTS

When observing the water runner robot utilizing a high speed camera (Phantom V7.0) at 3000 fps, we observed the formation of plumes of water dragged from the cavity to the edge of the foot during foot retraction [21]. This plume can be seen in Fig. 3. The plume results in excess splashing, additional drag on the foot, and may cause cavity deformation or collapse. At the very least, it represents an unnecessary expenditure of energy.

Fig. 3. Photograph of the water plume dragged from the cavity by the foot during the retraction phase of the robot's step.

Basilisk lizards close their feet during the recovery phase of their steps in the water, so nature may have already dealt with this problem. That being said, the basilisks still splash as they run, so the problem may be unsolvable.

There are three distinct possibilities as to the origin of the plume. First, it might simply be due to the foot passing through the cavity wall during retraction. This could be somewhat mitigated by feet which partially collapse during retraction to avoid scraping the cavity sidewalls. Second, there might be a vacuum action during the retraction that pulls the water up with the foot. To combat this, feet would have to allow air to flow to the foot/water interface to prevent water being pulled up with the foot. Lastly, there might be a hydrophilic interaction between the water and the material of the foot, giving the water a greater opportunity to cling to the foot during retraction. By using materials which are highly hydrophobic, this effect can be mitigated.

Several different foot designs were constructed and tested, and videos were made with a high speed camera. Through the testing, lift and drag were measured and compared to flat circular feet, which are used as a baseline. Through the high speed video footage, an attempt was made to determine which feet if any could completely avoid plume formation, and which feet created excessively large plumes. Also, by determining which feet were more effective in avoiding plume formation, the causes of the plume may be inferred. The different feet design were:

1. Compliant feet: circular feet which have folding joints on either side of the attachment with the leg. These joints fold only downward, and have a physical stop to prevent them from folding upwards. By using joints which can only fold in one direction, theoretically, feet would slap and stroke in a flat formation, fold during retraction, and avoid accidentally collapsing the cavity. Joints were placed both toward the front and back of the foot, and also on either side.

2. Elastic feet: compliant feet with a piece of elastic material connected across the folding joints to increase the effective spring stiffness of the flap bending. The stiffness of the joint was increased due to concerns that the flap response was slower than the 7 Hz running speed. Like compliant feet, joints were placed both toward the front and back of the foot, and also on either side.

3. Elliptical: feet with an elliptic shape instead of circular. By using feet with non-circular cross section, it was believed that the cavity collapse dynamics may change. This may affect plume formation and/or lift. The long axis was placed both running front to back and side to side.

4. Holed foot: circular feet with small holes in them. The diameter of the hole is chosen so that water does not pass through during the slap and stroke phases, but air can pass through during retraction. To calculate this diameter, the drag pressure is determined from (2) and used to find the force on a hole of diameter D. This is then compared to the surface tension force:

$$C_D^*[0.5\rho u_{max}^2 + \rho g h_{max}](.25\pi D^2) = \gamma\pi D \tag{8}$$

where u_{max} is the highest velocity of the downward stroke, approximately 1.65 m/s for the ankle from simulations, h_{max} is the lowest point of the foot below the water line, approximately 24 mm for the ankle from simulations, and γ

is the surface tension of water, 7.34×10^{-2} N/m [22]. While the maximum velocity and the lowest point of the stroke do not occur simultaneously, by using these maximum values a conservative maximum hole diameter of 0.26 mm was found.

5. Hydrophobic: circular feet with a hydrophobic coating of WX2100 ™, a fluorinated petroleum product, to make the feet more hydrophobic and shed water.

Figure 4 shows each of the different feet with characteristic dimensions noted. For circular, compliant, elastic, holed and hydrophobic feet, the foot's diameter was 40.0 mm. The major diameter on the elliptical foot was 50 mm and the minor diameter was 30 mm.

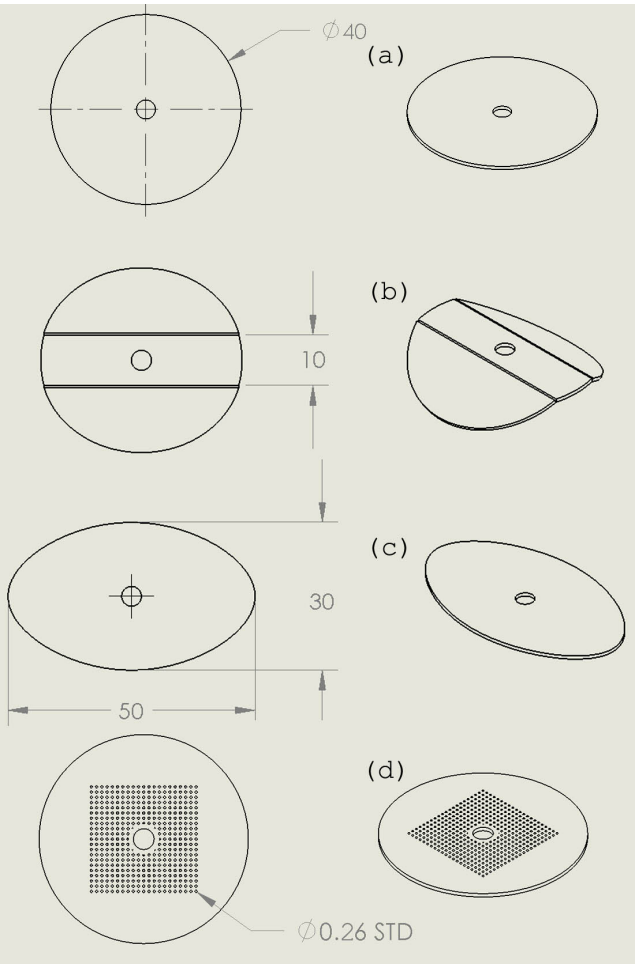

Fig. 4. Drawing of the different foot styles used in the experiments. (a) Geometry of the flat and hydrophobic feet. (b) Geometry of the compliant and elastic feet. (c) Geometry of the elliptic feet. (d) Geometry of the holed feet.

A. Analysis Procedure

During each test, the laser micrometer was turned on first and zeroed. A single leg of the robot was run at 7 Hz. After allowing several seconds for the system to reach steady state, data acquisition began. At least 10 seconds of data, representing at least 70 cycles, was obtained in each test run. After an acquisition, the system was stopped, the laser micrometer re-zeroed, and the test run again. The foot used by the robot was varied. For each foot design, at least 3 separate tests were run.

Acquired data was first visually inspected to ensure no outside disturbances occurred during the acquisition. Using MATLAB, a fast Fourier transform (FFT) was performed. To ensure the FFT functioned appropriately, the data was limited to a range which covered only an integer number of cycles. Also, the data was linearly interpolated to 2^N number of data points, strictly greater than the initial number of data points so that no data was discarded [17]–[19].

A program was run which identified the base frequency of the robot, approximately 7 Hz, and used this base frequency to find the next 10 harmonics. The magnitude and phase responses at these frequencies were identified and used to create a wave representative of a single cycle. At each frequency, the magnitude of the response was then scaled by the inverse of the system response at the same frequency. Phase lag at each frequency was removed from the phase response by adding the phase lag value. Once this was completed, the 11 components were summed to create a representation of the forces experienced by the water runner with the distortion introduced by the measuring system removed.

B. Results

The magnitude of the response for the first 11 harmonics, as well as the DC value for each type of foot are provided in Table I. The phase, in radians, of the response for those same harmonics are provided in Table II. In both tables, ^{1} denotes front and back and ^{2} denotes on the sides.

To determine the approximate time the foot spent in the air, stroking through the water, and retracting through the water, high speed footage of an elastic foot interacting with the water was closely examined [21]. Approximately 40% of each cycle is spent in the water, 50% in the air, and 10% retracting from the water. During foot removal, the folding portions of the foot snap back into position shortly after leaving the water. This creates a small upward spike in force with a very short duration. Using that point as reference, assuming that the retraction phase should have negative life, and the slap and stroke should have positive lift, the different sections of a step cycle were found and applied to the data from the elastic foot in Fig. 5. By extension, the cycles of all other feet were determined.

Examining the time response, one can quickly see that the flat, hydrophobic, and holed feet responses are quite similar, shown in Fig. 6. The hydrophobic foot performed, overall, slightly better, while the holed foot performed slightly worse. All three have a poor time-averaged response, with net negative lift. This is caused by the large negative force required to remove the foot from the water. In addition, there seems to be an additional dip in the force generated just before entering the water. This may be due to vibrations induced in the system from the large disparity between the peak lift and the peak drag when changing from the stroke phase to retraction.

For the elastic and compliant feet, lift and drag over time for all 4 variations are quite similar, as seen in Fig. 7. Both

Frequency	Air	Flat	Compliant^1	Compliant^2	Elastic^1	Elastic^2	Ellipse^1	Ellipse^2	Holed	Hydrophobic
DC	-0.0318	-5.0376	2.9053	3.1735	3.7737	3.0917	2.7007	-3.028	-5.4104	-3.1371
7	5.5769	12.5815	5.2741	5.6991	7.9986	5.3834	6.9918	13.6702	12.3957	12.3044
14	3.8	16.9591	10.2666	9.1888	11.2475	6.7751	12.7011	11.4894	15.6781	17.5394
21	13.1242	6.5469	8.888	6.7287	7.5337	7.7043	10.3149	9.4755	7.996	7.1952
28	3.6028	11.5368	2.4908	3.0408	2.5289	3.7797	1.259	7.543	10.3265	12.0134
35	0.8637	2.737	1.9871	1.4357	0.9889	2.664	1.0058	4.169	3.7658	2.7157
42	0.2671	2.8847	0.4173	0.8378	1.0419	0.8945	1.3886	1.6533	2.9744	2.9795
49	0.3945	1.2096	1.054	0.9267	1.0467	1.2208	0.7256	1.2506	1.4867	1.3775
56	0.4154	0.8666	0.288	0.0944	0.2535	0.1735	0.1397	0.4437	0.6994	0.8131
63	0.2229	1.7328	1.9688	1.6782	2.117	1.7396	1.4138	1.0637	1.4769	1.7358
70	0.6272	1.1718	0.5758	0.7784	0.8945	0.5903	0.4867	0.8257	2.0068	0.853
77	0.2406	1.3603	0.7422	0.6429	0.6084	0.4156	0.3127	0.4827	0.719	1.4367

TABLE I

MAGNITUDE OF RESPONSE IN FOURIER TRANSFORM (GRAMS). THE DC TERM IS THE AVERAGE LIFT.

Frequency	Air	Flat	Compliant^1	Compliant^2	Elastic^1	Elastic^2	Ellipse^1	Ellipse^2	Holed	Hydrophobic
7	-0.004	-0.004	-0.004	-0.004	-0.004	-0.004	-0.004	-0.004	-0.004	-0.004
14	1.097	-1.9998	-1.7204	-1.922	-2.449	-1.7705	-1.6727	-2.4319	-1.9996	-2.0336
21	-0.0029	1.0035	1.9119	1.2272	0.8598	1.6654	1.6462	1.2407	1.3155	0.8366
28	-0.9664	0.4208	1.1548	0.1531	-0.1177	1.0634	0.7013	-0.8233	0.3673	0.277
35	1.0469	2.9971	-1.5836	-2.6478	-2.8171	-2.0122	-2.7762	2.7094	-3.0006	2.709
42	2.8353	2.2599	-2.7736	1.5711	1.8712	2.8955	-1.8472	0.5316	1.8692	2.2228
49	2.7895	-2.1789	1.2223	-0.1859	-0.5338	0.2501	0.8172	-2.4286	-1.7887	-2.3274
56	-1.9358	-1.5677	-2.3405	-4.9819	-0.2908	-3.4461	-4.017	-3.999	-1.4347	-1.7905
63	-2.0565	-1.0301	-4.497	-1.0365	-1.9365	-6.0748	-2.131	-1.2743	-0.7548	-1.4468
70	-2.6467	-4.1509	-2.3897	-4.4557	-4.3506	-3.4115	-4.8845	-5.0638	-4.2705	-4.061
77	-2.64	-0.4775	-3.6168	-5.5017	-5.9565	-0.75	-6.2304	-2.2028	-0.313	-0.8408

TABLE II

PHASE OF RESPONSE IN FOURIER TRANSFORM (RAD)

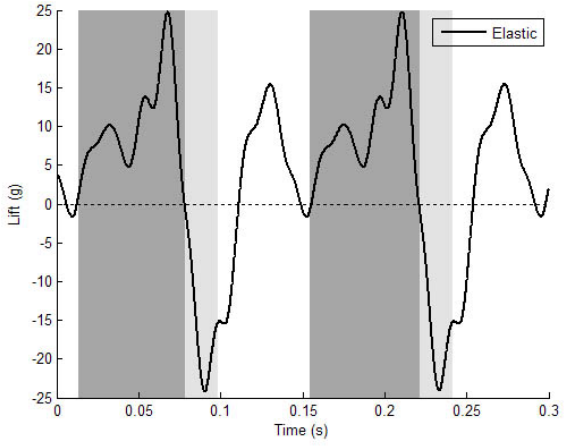

Fig. 5. Experimental time response of the elastic foot. White sections represent time spent in the air, darkly shaded sections represent the stroke phase, and lightly shaded sections represent foot retraction from the water. Lift is in grams.

the flap and elastic feet with flaps on the side have lower drag when retracting form the cavity. This may imply that the cavity walls to either side collapse before the cavity walls in line with the stroke direction.

For the ellipse feet, the front to back orientation provided far greater lift than the side to side orientation, shown in Fig. 8. The most notable reason for this difference in lift is the high pull out force experienced by the ellipse foot with major axis aligned side to side. This high pull out force supports the theory that cavity walls on the side collapse first.

A comparison between elastic, hydrophobic, and elliptical feet is shown in Fig. 9. Cavity drag for the hydrophobic foot, which had the greatest lift of the three circular feet, is much greater than in the other two designs. This is a possible explanation for the great plumes of water which are generated during retraction, as shown in Fig. 3. The peak lift for all feet is comparable. Compared to the other two, the hydrophobic foot also takes longer to return to zero lift after the retraction. Again, this is likely due to the large plumes generated, which were greatest for the circular, non-folding feet.

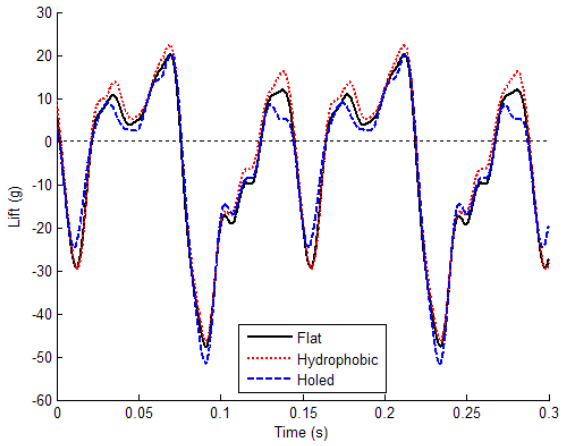

Fig. 6. Experimental time response of the flat, hydrophobic, and holed feet.

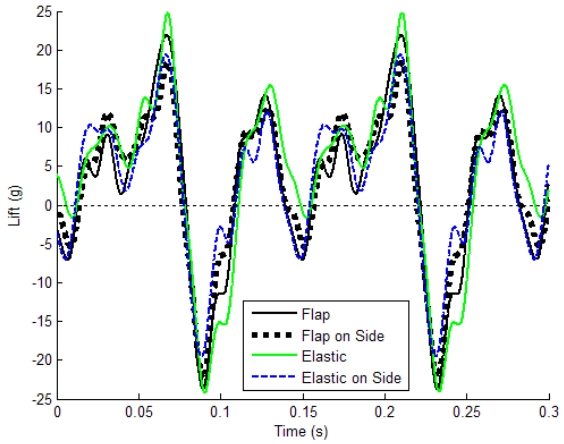

Fig. 7. Experimental time response of the flap and elastic feet. Flaps could either be arranged either front to back, or side to side relative to the leg.

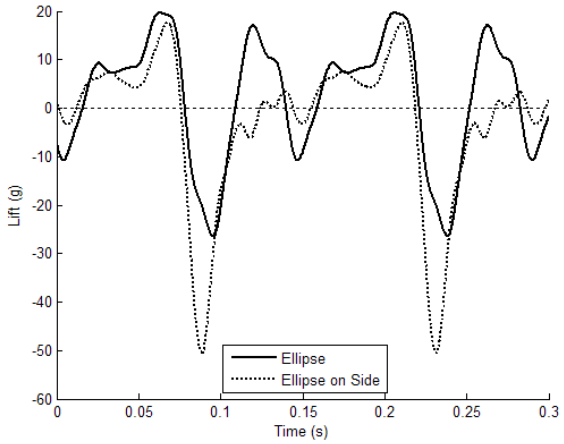

Fig. 8. Experimental time response of the ellipse feet. Major axis of the ellipse could be aligned front to back or side to side relative to the leg.

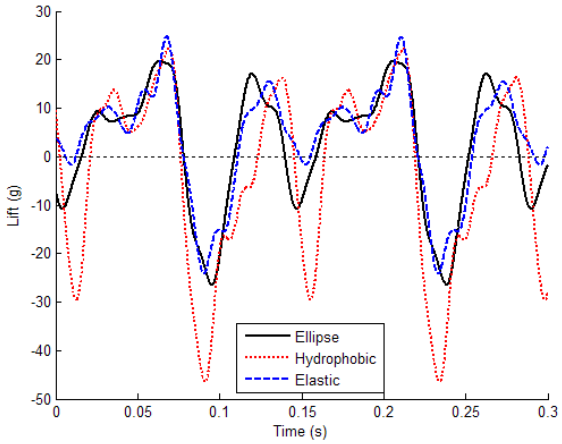

Fig. 9. Experimental time response of the elastic, hydrophobic, and elliptical feet. The ellipse foot is arranged with its major axis in line with the running direction. Also, the elastic foot has folding sections in front and back relative to the leg.

VI. DISCUSSION

Examining the DC response, one can quickly see that elastic feet are the best choices in terms of average lift. Overall, the high performance of the elastic and compliant feet suggest that the principle drag effect is caused by premature collapse of the cavity walls, and the feet which fold during the retraction phase are the best design choice. Further, the improved net lift of the ellipse, when compared with the standard flat foot implies that an elongated foot design is better than a circular foot. These two facts, taken together, suggest that an improved foot for the water runner would be both elongated, and have folding components. Such a foot would in fact be more like the basilisk lizard than the standard flat circle used in the previous water runner studies.

Feet with folding components on either side which collapsed during retraction experienced a smaller pull out force than similar feet with collapsing components on the front and back. In addition, elliptical feet with the major axis aligned side to side experienced a much greater pull out force than a similar foot with major axis aligned front to back. These two facts taken together seem to imply that cavity drag effects on the sides of the foot are greater than those in the front or back. But, overall lift was greatest when the collapsing component was aligned front to back. Perhaps a foot which can collapse in all directions would also be an improvement over current designs.

The test setup used in the above experiments had a single leg of the water runner slapping repeatedly in the same location for a contained volume of water approximately 30 cm wide. Waves generated by each impact event would hit the side walls and return, diminished, to the point of impact during the next step. For any water runner operating in the real world, the robot will travel forward with each step, and these returning waves are not likely to occur.

Additionally, problems associated with cavity drag during

retraction may be somewhat decreased when the water runner can move forward and the foot pulls out from the cavity more along the entry path. In that case, the non-folding, circular feet were unfairly punished in terms of lift due to the stationary nature of the test setup. Future test rigs may allow forward motion, or may flow water past a stationary system to simulate forward movement of the water runner.

Lastly, due to the harmonic motion of the system, the entire testing rig drops low into the water whenever the foot is not providing lift. This has the effect of increasing the measured drag of all the foot designs tested. Four legged water runners, which are constantly producing lift with one or more legs, will not experience this problem, so the net lift provided by four feet of a given design working in tandem will be greater than four times the effect of a single foot.

VII. CONCLUSION

Different foot designs for a water runner robot were tested to determine which had the best lift and drag characteristics. Feet with folding sections aligned front to back which remain flat during the slap and stroke phase and which collapse during retraction from the water were found to provide the largest lift and create the least drag. All feet with directionally compliant flaps which collapse during retraction performed better than feet which in no way collapsed during retraction. Compared to flat circular feet, ellipse shaped feet with their major axis aligned with the water runner's leg generated greater lift.

Future work on the water runner will be toward improving overall efficiency, adding steering and control systems, and making the robot amphibious. Efficiency is currently low because of the unavailability of low cost, light-weight, and efficient motors. The 9 g motors used by the current robot only have efficiencies on the order of 50%, with nearly 0.7 Watt of loss in the gearbox at running speeds of 7 Hz (no load). Any steering mechanism that is added must be light-weight and should not interfere with the the synchrony of each leg pair. Possibilities include adding a joint in the middle of the robot so that the front and back legs would have different lines of action, or shifting the center of mass by moving the battery box. To make the robot amphibious, designs are being tested which include energy storing springs for land locomotion. The ultimate goal is a fully autonomous and amphibious water runner capable of traversing both land and water.

Some issues that will have to be addressed are those dealing with the interaction of mechanical and electrical components with water. All wiring and exposed electronics must be shielded from the water for safety purposes and to prevent harmful shorts from damaging any of the systems. Motors especially must be water proof, or in water proof containers. Mechanical parts must be rust proof and preferably would be either hydrophobic or have a hydrophobic surface treatment. This would prevent loss of lift due to the accumulation of water on the robot's surface. Also, light-weight, high current density batteries must be chosen to reach the performance anticipated by simulations. Lastly, light-weight, high strength materials must be used for any load bearing components.

VIII. ACKNOWLEDGMENTS

The authors would like to thank the NanoRobotics Laboratory members for their support and suggestions.

REFERENCES

[1] R. Suter et al., "Locomotion on the Water Surface: Propulsive Mechanisms of the Fisher Spider *Dolomedes Triton*," *J. of Exp. Biology*, vol. 200, pp. 2523-2538, 1997.

[2] D. Hu, B. Chan, and J. Bush, "The hydrodynamics of water strider locomotion," *Nature*, vol. 424, pp. 663-666, 2003.

[3] D. Hu and J. Bush, "Meniscus-climbing Insects," *Nature*, vol. 437, pp. 733-736, 2005.

[4] J. Bush and D. Hu, "Walking on Water: Biolocomotion at the Interface," *Annu. Rev. of Fluid Mech.*, vol. 38, pp. 339-369, 2006.

[5] S. Hsieh, "Three-dimensional hind limb kinematics of water running in the plumed basilisk lizard (*Basiliscus plumifrons*)," *The Journal of Experimental Biology*, vol. 206, pp. 4363-4377, 2003.

[6] J. Glasheen and T. McMahon, "Vertical water entry of disks at low Froude number," *Phys. Of Fluids*, vol. 8, pp. 2078-2083, 1996.

[7] J. Glasheen and T. McMahon, "Size-Dependence of Water-Running Ability in Basilisk Lizards (*Basiliscus Basiliscus*)," *The Journal of Experimental Biology*, vol. 199, pp. 2611-2618, 1996.

[8] J. Glasheen and T. McMahon, "A hydrodynamic model of locomotion in the Basilisk Lizard," *Nature*, vol. 380, pp. 340-342, 1996.

[9] T. Hsieh and G. Lauder, "Running on water: Three-dimensional force generation by basilisk lizards," *PNAS*, vol. 101, pp. 16784-16788, 2004.

[10] A. Boxerbaum, P. Werk, D. Quinn, and R. Vaidyanathan, "Design of an Autonomous Amphibious Robot for Surf Zone Operation," *Proceedings of the IEEE/ASME International Conference on Advanced Intelligent Mechatronics*, pp. 1459-1464, 2005.

[11] A. Crespi, A. Badertscher, A. Guignard, and A. Ijspeert, "AmphiBot I: an amphibious snake-like robot," *Robotics and Autonomous Systems*, vol. 50, pp. 163-175, 2005.

[12] S. Guo, T. Fukuda, and K. Asaka, "A New Type of Fish-Like Underwater Microrobot," *IEEE/ASME Transactions on Mechatronics*, vol. 8, pp. 136-141, 2003.

[13] C. Georgiadis *et al*., "AQUA: An aquatic walking robot," *Proceedings of the IEEEE/RSJ International Conference on Intelligent Robots and Systems (IROS)*, pp. 3525-3531, 2004.

[14] Y. Song, S. Suhr, and M. Sitti, "Modeling of the Supporting Legs for Designing Biomimetic Water Strider Robots," *Proceedings of International Conference on Robotics and Automation (ICRA)*, pp. 2303-2310, 2006.

[15] H. Takonobu, K. Kodaira, and H. Takeda, "Water Striders Muscle Arrangement-based Robot," *IEEE/RSJ International Conference on Intelligent Robots and Systems (IROS)*, pp. 1754-1759, 2005.

[16] S. Floyd, T. Keegan, J. Palmisano, and M. Sitti, "A Novel Water Running Robot Inspired by Basilisk Lizards," *IEEE/RSJ International Conference on Intelligent Robots and Systems (IROS)*, pp. 5430-5436, 2006.

[17] R. Bracewell, "The Fourier Transform and Its Applications, 2nd Ed.," WCB/McGraw-Hill, 1986.

[18] D. C. Champeney, "Fourier Transforms and Their Physical Applications," Academic Press, 1973.

[19] W. Briggs and V. E. Henson, "The DFT: An Owners Manual for the Discrete Fourier Transform," Society for Industrial and Applied Mathematics, 1995.

[20] B. H. Tongue, "Principles of Vibration, 2nd Ed.," Oxford University Press, 2002.

[21] [Online] Available: http://nanolab.me.cmu.edu/projects/waterrunner/

[22] B. Munson, D. Young, and T. Okiishi, "Fundamentals of Fluid Mechanics 4th Ed.," John Wiley and Sons Inc., 2002.